# Materials Advances

Accepted Manuscript

This article can be cited before page numbers have been issued, to do this please use: T. T. Hoang, A. T. Le, H. T. Dang and H. N. Duong, *Mater. Adv.*, 2026, DOI: 10.1039/D5MA00802F.




ROYAL SOCIETY OF CHEMISTRY

rsc.li/materials-advances

View Article Online
DOI: 10.1039/D5MA00802F

# GREEN SYNTHESIS OF CQD/AGNPS COMPOSITE FROM GUAVA LEAF AND ITS POTENT ANTIMICROBIAL ACTIVITY AGAINST MULTIDRUG-RESISTANT ESKAPEE PATHOGENS

Hoang Thi Thu[1] , Le Tuan Anh [2], Dang Thien Huong [3] Duong Ngoc Huyen[1],

1- Industrial University of Ho Chi Minh City, Ho Chi Minh City, Viet Nam.

2- School of Pharmacy, University of Medicine and Pharmacy at Ho Chi Minh city, Viet Nam.

3-Lawrence S.Ting School, 1 Raymondienne Street, Tan My Ward, Ho Chi Minh City, Vietnam.

**Corresponding author:**

**Hoang Thi Thu, Ph.D**

Faculty of Fundamental Science

Industrial University of Ho Chi Minh City, Ho Chi Minh City, Viet Nam.

Email: hoangthithu@iuh.edu.vn, hoangthukhcn@gmail.com; Tel: +84986062980

**Abstract:**

This study presents a green synthesis approach for fabricating CQD/AgNPs nanocomposite materials, in which carbon quantum dots (CQDs) were derived from dried guava leaves (*Psidium guajava*)—a widely available, low-cost, and accessible plant material in Vietnam. The resulting nanocomposite was characterized using a range of advanced techniques including UV–Vis, PL, XRD, FTIR, Raman, SEM and TEM. These analyses confirmed the formation of uniformly dispersed, spherical nanoparticles with an average diameter of approximately 33.4 nm and good structural stability. Interestingly, the CQD/AgNPs nanocomposite demonstrated strong antibacterial activity against multidrug-resistant (MDR) pathogens of the ESKAPEE group. In particular, the material exhibited a minimum inhibitory concentration (MIC) of 25 µg $mL^{-1}$ towards *Acinetobacter baumannii*, a highly drug-resistant bacterium commonly associated with hospital-acquired infections. The nanocomposite also showed significant inhibitory effects against ciprofloxacin-resistant strains of *Staphylococcus aureus*, *Klebsiella pneumoniae, Pseudomonas aeruginosa*, and *Enterobacter* spp., with MIC values of 50 µg $mL^{-1}$.

This report is among the first to develop a green-synthesized CQD/AgNP nanomaterial with low production cost, good industrial scalability, and long-term stability at room temperature. Additionally, the study also comprehensively evaluates the material's

View Article Online
DOI: 10.1039/D5MA00802F

antibacterial activity against five drug-resistant ESKAPEE pathogens, thereby highlighting its potential application as an alternative to conventional antibiotics.

**Keywords:**

*Carbon quantum dots, silver nanoparticles, green synthesis, antibacterial, ESKAPE, ESKAPEE, nanocomposite, multi-drug resistant bacteria, guava.*





## 1. Introduction

The global rise in infections caused by multidrug-resistant (MDR) pathogens, particularly the ESKAPEE group (*Enterococcus faecium, Staphylococcus aureus, Klebsiella pneumoniae, Acinetobacter baumannii*, *Pseudomonas aeruginosa*, *Enterobacte*r spp., and *Escherichia coli*), poses a significant threat to public health systems worldwide (1,2). The widespread misuse and overuse of antibiotics in both clinical and agricultural settings have accelerated the evolution of resistance mechanisms, thereby diminishing the efficacy of conventional antimicrobial therapies (3). In the European Union and European Economic Area (EU/EEA), antimicrobial-resistant infections are estimated to cause over 35,000 deaths annually—a number that continues to rise each year (4). Among the ESKAPEE group, *Klebsiella pneumoniae* and *Acinetobacter baumannii* have raised major concerns. According to the 2023 EARS-Net report, the incidence of bloodstream infections caused by carbapenem-resistant *K. pneumoniae* in the European Union reached 3.97 cases per 100,000 population, increasing 57.5 percent compared to 2019. Notably, infections caused by carbapenem-resistant *A. baumannii* rose by over 121% between 2018 and 2021, with the majority of isolates also exhibiting resistance to fluoroquinolones and aminoglycosides (ECDC, 2023). These findings highlight the growing threat of extensively drug-resistant bacteria and emphasize the urgent need for new, effective, and sustainable antibacterial strategies (5–7).

Nanotechnology, particularly the use of silver nanoparticles (AgNPs), has attracted considerable attention in the search for alternative antimicrobial solutions (8,9). AgNPs exhibit broad-spectrum activity and act through multiple mechanisms, demonstrating strong efficacy against both Gram-positive and Gram-negative bacteria (8,10,11). However, conventional synthesis methods often rely on toxic reducing agents such as sodium borohydride, sodium hydroxide, hydrochloric acid or hydrazine, raising concerns regarding environmental safety, biocompatibility, and feasibility for practical applications.

View Article Online
DOI: 10.1039/D5MA00802F





To overcome these limitations, green synthesis approaches have emerged as a promising alternative. By employing plant extracts, polysaccharides, or natural polymers as both reducing and stabilizing agents, these methods offer a more sustainable and environmentally friendly route for the production of AgNPs (12–17). Numerous studies have reported the strong antimicrobial performance of biosynthesized AgNPs, reinforcing their potential for biomedical and environmental applications. For instance, the study by Trieu et al. (2025) [18] demonstrated that AgNPs synthesized using Psidium guajava (guava) leaf extract exhibited potent antibacterial activity against both Gram-positive (Staphylococcus aureus, Enterococcus faecalis) and Gram-negative (Pseudomonas aeruginosa) species. Similarly, Chartarrayawadee et al. (2020) synthesized AgNPs via a green route using an extract from Lysimachia foenum-graecum Hance. The resulting nanoparticles showed prolonged colloidal stability and strong antibacterial activity against S. aureus, with an inhibition zone diameter of 19.08 ± 0.67 mm—exceeding that of the positive control, chloramphenicol (13). More recently, Raza et al. (2023) developed "TeaNPs" using three types of tea infusions (black, green, and red) and found that green tea-derived nanoparticles (GTeaNPs) were the most active, eliminating up to 80 % of Gram-negative bacterial cells within 3 h at 100 μg $mL^{-1}$—significantly outperforming ampicillin under the same conditions (18).

Although green-synthesized AgNPs have demonstrated strong and broad-spectrum antibacterial activity, certain drawbacks remain, including the need for refrigerated storage (≈ 4 °C) and relatively high MIC values, which hinder practical application. Recently, combining AgNPs with carbon quantum dots (CQDs) has gained attention as an effective strategy to enhance antibacterial efficiency while maintaining environmental safety. CQDs can act as both reducing and stabilizing agents during AgNP formation and improve bacterial adhesion, thereby enhancing antibacterial efficacy through a synergistic mechanism (19–21).

Carbon quantum dots (CQDs) are a class of carbon-based nanomaterials known for their environmental friendliness, high photostability, and strong electron-transfer capability (22–25). They can be readily synthesized from a wide range of biomass sources, including leaves, fruit peels, and agricultural residues (26). Common synthetic routes include hydrothermal treatment, microwave-assisted processes, and high-temperature carbonization (23,27–30). These methods offer low cost, operational simplicity, and good scalability (24,26). CQDs also exhibit mild antibacterial activity due to the reactive surface

View Article Online
DOI: 10.1039/D5MA00892F

functional groups (31). In addition, they provide slight wound-healing support, which is associated with their antioxidant properties and high biocompatibility (19,32,33).

In this study, we report the fabrication of a CQD/AgNPs nanocomposite using an environmentally friendly physical approach that yields a stable product at room temperature and is suitable for large-scale production. Furthermore, the antibacterial activity of the synthesized nanocomposite was comprehensively evaluated against clinically relevant multidrug-resistant (MDR) ESKAPEE pathogens, providing valuable insights for the practical development of eco-friendly antimicrobial agents.

## 2. Materials and methods

### 2.1. Materials

Guava leaves were collected and dried. Polyvinyl alcohol PVA-124 (China) and silver nitrate ($AgNO_3$, Prolabo – France) were used in the synthesis. Dialysis tubing with a cut-off of 2000 Da was purchased from Spectrum Lab (USA).

For antibacterial testing, nutrient broth (NB) and nutrient agar (NA) were purchased from Oxoid Ltd. (Basingstoke, Hampshire, UK).

The multidrug-resistant (MDR) bacterial strains used in this study included Acinetobacter baumannii VS73, Escherichia coli ND01, methicillin-resistant Staphylococcus aureus (MRSA) VS02, Klebsiella pneumoniae VS39, and Pseudomonas aeruginosa ND26. These strains were isolated from clinical samples by the Department of Microbiology–Parasitology, Faculty of Pharmacy, University of Medicine and Pharmacy at Ho Chi Minh City, Vietnam.

All strains were stored in glycerol at –80°C. Before testing, they were revived by streaking onto Mueller–Hinton agar plates and incubated overnight at 37°C. Then, 2–3 colonies of each strain were picked and suspended in PBS until the optical density at 600 nm reached 0.08–0.1, equivalent to about $10^8$ CFU/mL. This bacterial suspension was further diluted with PBS to around $10^6$ CFU/mL and used within 15 minutes after preparation.

Ciprofloxacin disks were obtained from Bio Techem Co., LTD (Vietnam). Other available chemicals were purchased from El-Gomhouria for Trading Chemicals and Medical Appliances (Alexandria, Egypt) and used without further purification.

### 2.2. Carbon Quantum Dots (CQDs-G) Synthesis

View Article Online
DOI: 10.1039/D5MA00802F

Three grams of dried guava leaves were added to a 200 mL stainless steel cup and carbonized at 800 °C in a muffle furnace. After 15 minutes, the sample was rapidly cooled by removing it from the furnace and pouring in 50 mL of distilled water. Pour the mixture into an autoclave, seal the lid tightly, and place the autoclave in a furnace. Set the furnace to 400°C and heat for 10 h. After that, wait for the furnace to cool completely to room temperature before proceeding. The mixture was stirred with a magnetic stirrer for 30 minutes, microwaved for 5 minutes, and then left to settle for 2 days. It was roughly filtered through 47 μm filter paper, then transferred to a dialysis bag (molecular weight cutoff: 2000 Da) and dialyzed in distilled water for 3 days. The final solution was gently heated at 70 °C until the volume is roughly 20 mL, which was then used to synthesize the CQD/AgNPs nanocomposite.

### 2.3. CQD/AgNPs Nanocomposite Synthesis

#### Preparation of CQD/AgNPs Nanocomposite

The green synthesis process of CQD/AgNPs is illustrated in Figure 1, began with the dilution of 5 mL of the previously prepared CQD solution was diluted with 420 mL of distilled water, resulting in a total volume of 425 mL. At the same time, 0.835 g of silver nitrate ($AgNO_3$) was dissolved in 25 mL of distilled water to obtain a 0.01 mol solution. Consequently, this $AgNO_3$ solution was added dropwise to the CQDs solution under constant magnetic stirring. The mixture was then adjusted to a final volume of 500 mL with distilled water and stirred at room temperature for 1 hour to promote the interaction between $Ag^+$ ions and the CQDs.

Meanwhile, 1 g of polyvinyl alcohol (PVA) was dissolved in 500 mL of distilled water under magnetic stirring at room temperature to obtain a homogeneous 0.2% (w/v) PVA solution. The $AgNO_3$/CQDs mixture (500 mL) was then added into the PVA solution while maintaining stirring. The final mixture (1000 mL) was stirred for an additional hour to ensure uniform dispersion of silver ions and CQDs in the PVA matrix.

Eventually, the solution was transferred to PET containers and exposed to gamma irradiation at 25 kGy using a Co-60 source (referred to as sample M1). Gamma irradiation facilitates the in-situ formation and even distribution of AgNPs and CQDs while embedding them within the PVA network, helping to reduce aggregation. This approach does not require chemical reducing agents or surfactants, aiming for a greener and more efficient synthesis of stable CQD/AgNPs nanocomposites.

View Article Online
DOI: 10.1039/D5MA00802F

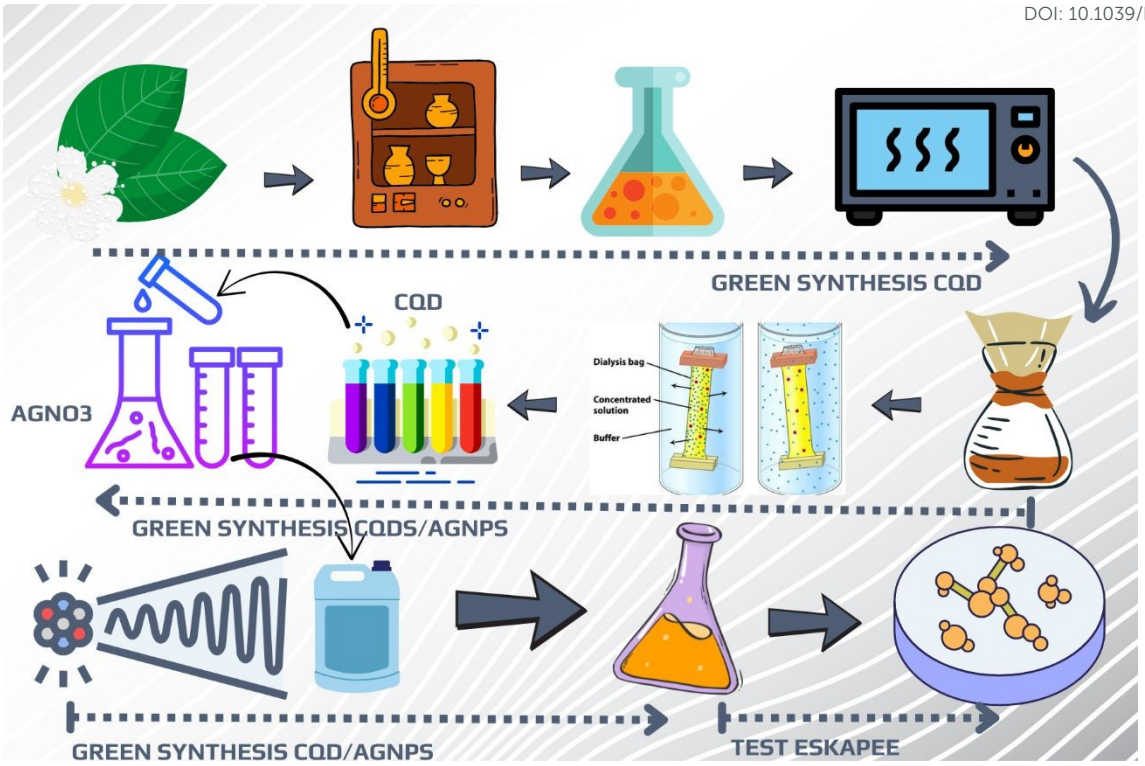


*Figure 1: Green synthesis process of CQD/AgNPs nanocomposite.*

## Material characterization and instrumentation

The UV–Vis absorption spectra of the samples in aqueous solution were recorded using a Jasco V530 UV–Vis spectrophotometer. The morphology and crystal structure were characterized by scanning electron microscopy (SEM, HITACHI SU8100), transmission electron microscopy (TEM, JEOL JEM-1400), and X-ray diffraction (XRD, D8 ADVANCE with CuKα radiation, λ = 1.54 Å), respectively. Fourier-transform infrared (FT-IR) spectra were obtained using an Equinox 55 FT-IR spectrometer.

## Antibacterial Activity Assay

The antibacterial activity of the CQD/AgNP nanocomposite was evaluated using the agar well diffusion method. Multidrug-resistant (MDR) strains from the ESKAPEE group, including *Acinetobacter baumannii* VS73, *Escherichia coli* ND01, *Staphylococcus aureus* (MRSA) VS02, *Klebsiella pneumoniae* VS39, and *Pseudomonas aeruginosa* ND26, were selected for testing. Bacterial suspensions were prepared as previously described and uniformly spread over Mueller–Hinton agar (MHA) plates using sterile cotton swabs to ensure even distribution.

Sterile wells with a diameter of 6 mm were aseptically punched into the agar plates, and 50 µL of the test sample was added to each well. The plates were then incubated at 37 °C

View Article Online
DOI: 10.1039/D5MA00802F

for 18–24 hours to allow the sample to diffuse and interact with bacterial cells in the surrounding agar medium. After incubation, antibacterial activity was determined by measuring the diameter (in mm) of the inhibition zones around the wells, indicating the area where bacterial growth was suppressed. A ciprofloxacin disc (30 µg) was used as a positive control to compare the antimicrobial efficacy with that of a clinically used antibiotic, while sterile distilled water served as a negative control to verify the accuracy of the experimental setup.

**Minimum Inhibitory Concentration (MIC) Evaluation**

The minimum inhibitory concentration (MIC) of the CQD/AgNPs nanocomposite was determined using the broth microdilution method, following the guidelines of the Clinical and Laboratory Standards Institute (CLSI). The samples were diluted two-fold in Mueller–Hinton Broth (MHB) to create a range of concentrations. Subsequently, 100 µL of each dilution was added to individual wells of a sterile 96-well plate.

Afterward, 5 µL of bacterial suspension (~$10^7$ CFU/mL) from the MDR strains was added to each well. The plates were then incubated at 37 °C for 24 hours without shaking.

After incubation, the wells were observed directly against a dark background. The MIC was recorded as the lowest concentration where no visible bacterial growth was detected. All tests were performed in triplicate for each strain to ensure consistency and reliability.

**Cytotoxicity Assay**

The cytotoxicity of the synthesized CQD/AgNPs nanocomposite was evaluated using the standard MTT assay on human embryonic kidney (HEK293A) cells to assess its biocompatibility. The cells were cultured in 96-well plates and treated with different concentrations of the nanocomposite (100, 50, 25, 12.5, and 6.25 µg $mL^{-1}$) for 24 h. After incubation, MTT reagent was added, and the absorbance of the resulting formazan product was measured at 570 nm using a microplate reader. Cell viability was calculated relative to the untreated control according to standard protocols.

## 3. Results and Discussion

### 3.1. Characterization of CQD/AgNPs Composite

(a)

View Article Online
DOI: 10.1039/D5MA00802F

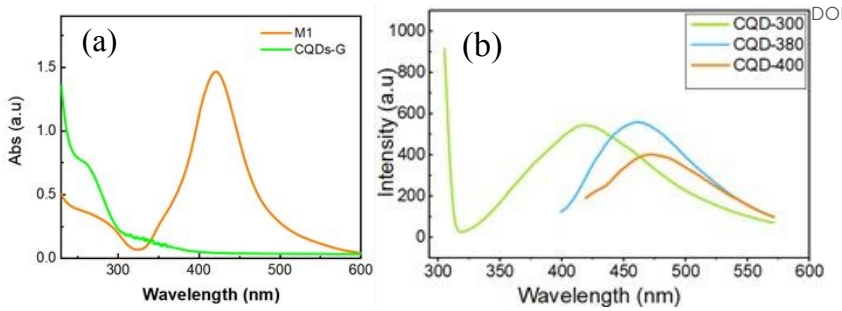


*Figure 2: UV–Vis spectrum of CQDs (CQDs-G) and CQD/AgNPs nanocomposite (M1) (a). Photoluminescence (PL) spectra of CQDs recorded under different excitation wavelengths (300, 380, and 400 nm) (b).*

The UV–Vis absorption spectrum of the CQD/AgNPs composite material (sample M1), as presented in Fig. 2a, exhibits a distinct surface plasmon resonance (SPR) peak at approximately 420 nm. This characteristic peak strongly indicates the formation of silver nanoparticles (AgNPs), as it corresponds to the collective oscillation of conduction electrons on the nanoparticle surface when excited by light. The narrow and symmetrical shape of the SPR band suggests that the synthesized AgNPs are mostly spherical and have a relatively uniform size distribution. The presence of the SPR band confirms the formation of AgNPs, which is consistent with previous studies (12–14). In addition to the SPR feature, a small shoulder appears in the 300–350 nm region, likely associated with n → π transitions or intrinsic electronic transitions in the carbon core of the carbon quantum dots (CQDs), indicating the coexistence of both CQDs and AgNPs in the nanocomposite. The absence of significant peak broadening or red shift suggests good colloidal stability and minimal aggregation of AgNPs in the presence of CQDs.

To further investigate the optical characteristics of the synthesized CQDs, the photoluminescence (PL) spectra were recorded at different excitation wavelengths (300, 380, and 400 nm), as shown in Figure 2b. The emission intensity and peak position varied with the excitation wavelength, showing a gradual red-shift from approximately 425 nm to 469 nm as the excitation wavelength increased. This excitation-dependent emission is a typical feature of carbon quantum dots and is generally attributed to multiple emissive surface states and defect-related energy traps. The strong blue emission and relatively short wavelength of the main PL peak suggest that the as-synthesized CQDs possess a small particle size with narrow size distribution. Such behavior reflects the heterogeneous surface structure and confirms the excellent optical tunability of the CQDs, suggesting their strong potential for bioimaging and optoelectronic applications (22,25,34). However, this estimation is qualitative and based solely on optical observations; the actual particle size

View Article Online
DOI: 10.1039/D5MA00802F

and morphology of the CQDs will be further verified by transmission electron microscopy (TEM) analysis.

To examine the crystalline structure of the CQD/AgNPs nanocomposite, X-ray diffraction (XRD) analysis was conducted, as shown in Fig. 3. The diffraction pattern revealed distinct peaks at 2θ ≈ 38.1°, 44.3°, 64.4°, and 77.4°, corresponding to the (111), (200), (220), and (311) planes of face-centered cubic (fcc) silver, according to JCPDS card no. 04-0783. Using the Debye–Scherrer equation, the average crystallite size of the silver nanoparticles was estimated to be approximately 30 nm. The most intense diffraction peak at 38.1° suggests a preferred orientation along the (111) plane, which is commonly observed in AgNPs synthesized through biological or green methods. The XRD pattern confirms the presence of AgNPs with fcc structure and indicates good crystallinity and effective particle formation during synthesis, consistent with previous reports on plant-extract-based AgNPs (12,14,20)

In the synthesized sample, no characteristic peaks of silver oxide impurities ($Ag_2O$, AgO) were observed, indicating that the reduction of $Ag^+$ ions to metallic $Ag^0$ was complete.

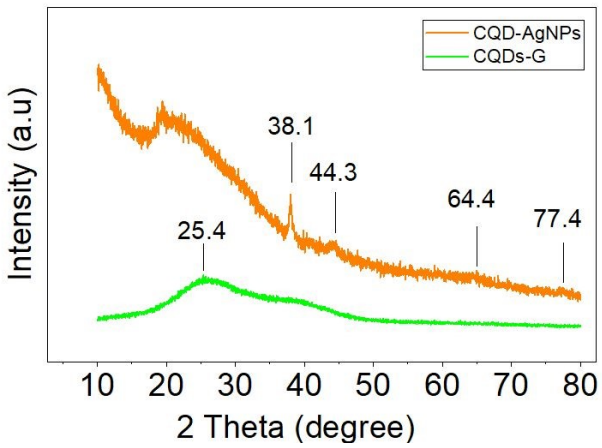


*Figure 3: XRD pattern of CQDs and CQD/AgNPs nanocomposite (M1) showing crystalline AgNPs peaks and amorphous CQD background*

In addition to the diffraction peaks associated with silver, a broad, low-intensity region was observed around 2θ ≈ 20–25°. This feature is characteristic of the amorphous structure of carbon quantum dots (CQDs), which has also been reported in previous studies using biomass-derived CQDs (23,24,27).

Altogether, these results suggest that the CQD/AgNPs nanocomposite consists of highly crystalline silver nanoparticles evenly dispersed within an amorphous carbon background, confirming the successful synthesis of this hybrid material. Moreover, to further assess the

View Article Online
DOI: 10.1039/D5MA00802F

particle size and distribution, TEM, SEM analysis of CQDs, CQD/AgNPs were performed (Fig 4).

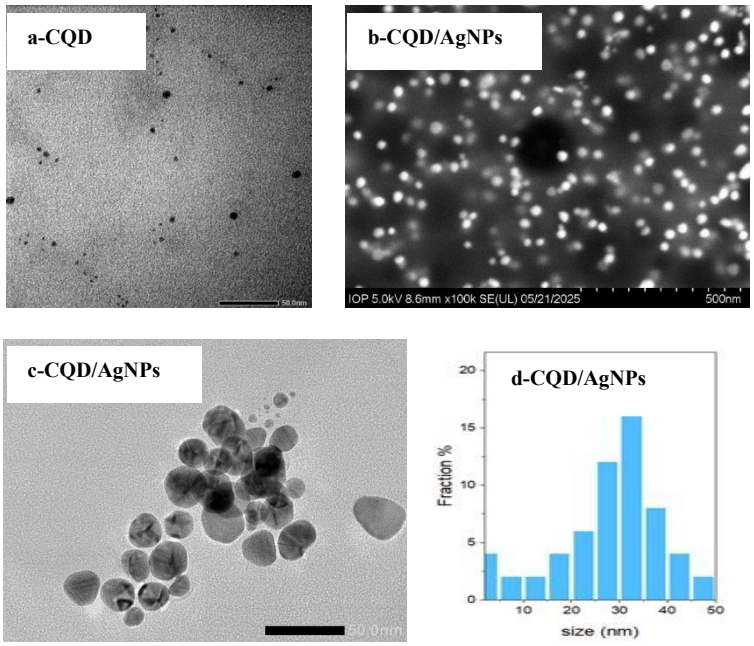


*Figure 4: TEM image of CQDs-G (scale 50nm - a), SEM image of the CQD/AgNPs nanocomposite (M1) at 500nm scale showing well-dispersed spherical AgNPs on the carbon quantum dot matrix (b), TEM image of CQD/AgNPs (scale bar = 50 nm) (c) and particle size distribution of CQD/AgNPs (d).*

As presented in Fig. 4a, the TEM image indicates that the synthesized CQDs are uniformly dispersed, nearly spherical in shape, and range from 1 to 6 nm in diameter, with an estimated average size of about 4.2 nm.

Furthermore, the SEM image of the CQD/AgNPs (Fig. 4b) nanocomposite reveals well-dispersed, nearly spherical nanoparticles without noticeable aggregation, suggesting that the CQD matrix effectively prevents agglomeration and contributes to the structural stability of the composite.

In addition, the TEM image and particle size distribution of the CQD/AgNPs nanocomposite (Fig. 4c,d) provide further confirmation, showing uniformly distributed nanoparticles with an average size of approximately 33.4 nm, which is slightly larger than the crystallite size estimated from XRD. This minor discrepancy is likely due to the presence of an amorphous carbon layer encapsulating the Ag nanoparticles, as also reported in several previous studies (20,35).

Overall, the close correlation among the XRD, SEM, and TEM analyses clearly confirms the successful synthesis of well-crystallized, uniformly dispersed AgNPs stabilized within the CQD framework. Such a homogeneous nanostructure is expected to play a crucial role

View Article Online
DOI: 10.1039/D5MA00802F

in enhancing the colloidal stability and antimicrobial performance of the CQD/AgNPs composite.

FTIR analysis was conducted to investigate the chemical composition and surface functional groups of the CQD/AgNPs nanocomposite. As shown in Fig. 5, broad absorption bands in the range of 3300-3500 $cm^{-1}$ are attributed to the presence of surface hydroxyl (C–OH) and amine ($–NH_2$) groups. The absorption band observed at approximately 1644 $cm^{-1}$ is assigned to C=C stretching vibrations within aromatic rings. Moreover, the sharp bands at 611 and 720 $cm^{-1}$ correspond to out-of-plane bending vibrations of aromatic C–H bonds. In the CQD/AgNPs nanocomposite, the absorption band at 1644 $cm^{-1}$ is also associated with quinone or conjugated carbonyl (C=O) groups, indicating structural modifications of CQDs during the reduction process. These findings suggest that the coal-derived CQDs possess an aromatic carbon framework with abundant surface amino and phenolic hydroxyl groups, which collectively serve as electron donors for reducing $Ag^+$ ions into elemental silver ($Ag^0$).

In addition to their reductive function, these surface functional groups also play a vital role in modulating the antimicrobial behavior of the CQD/AgNPs nanocomposite. The –COOH, –OH, and $–NH_2$ groups enhance the adhesion and electrostatic interaction between the nanocomposite and bacterial cell membranes, improving surface contact and facilitating the release of $Ag^+$ ions as well as the generation of reactive oxygen species (ROS) (19,20). Such interactions increase membrane permeability and promote the penetration of AgNPs into bacterial cells, ultimately contributing to the enhanced antibacterial activity of the CQDs/AgNPs composite.

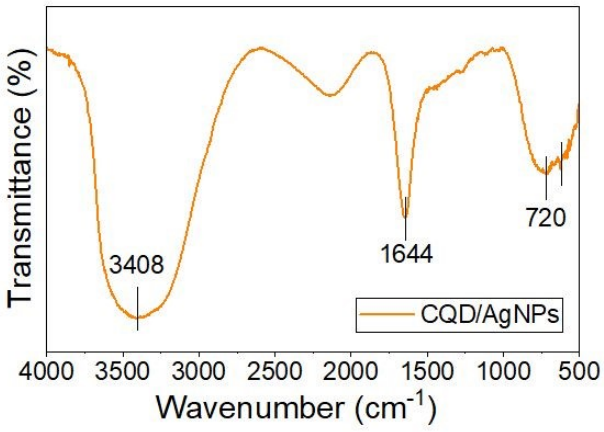


*Figure 5: FTIR of CQD/AgNPs*

View Article Online
DOI: 10.1039/D5MA00802F

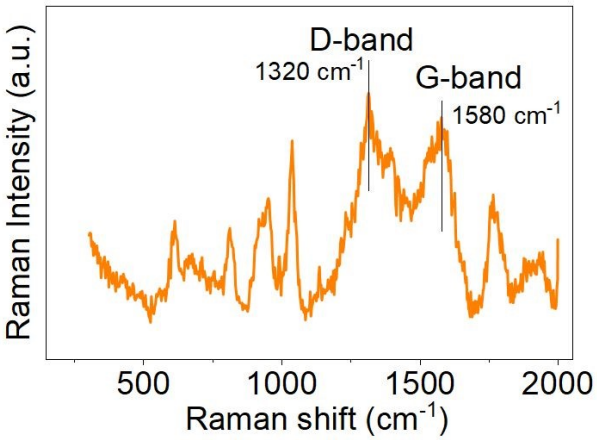


*Figure 6 Raman spectrum of CQD/AgNPs*

The structural characteristics of CQD/AgNPs were further validated through Raman spectroscopic analysis. As illustrated in Fig. 6, the Raman spectrum displays two prominent peaks located at 1320 $cm^{-1}$ and 1580 $cm^{-1}$, which are attributed to the D and G bands of graphitic carbon, respectively (36–38). The calculated ID/IG ratio of 1.03 indicates a predominantly amorphous structure with a high degree of disorder. This ratio also reflects the relative abundance of $sp^3$ to $sp^2$ hybridized carbon, suggesting the presence of structural imperfections within the green synthesized CQDs. In addition to the characteristic D and G bands, several sharper Raman peaks can be observed in the 1000–1600 $cm^{-1}$ region. These additional peaks may originate from the vibrational modes of organic functional groups such as C–H, C=O, and C–N, which are derived from residual biomolecules of the guava-leaf precursor that remain adsorbed on the nanocomposite surface. Similar Raman features have been reported for biologically synthesized AgNPs that are coated with or interact with polyphenolic compounds (36,37). The presence of these surface organic species is also consistent with the FTIR results, indicating that these functional groups contribute to improving the dispersion and colloidal stability of the CQDs/AgNPs system in aqueous solutions.

In summary, the structural analyses from Raman spectroscopy, together with SEM, TEM, XRD, UV–Vis, and FTIR measurements, confirm the successful synthesis of a stable and uniform CQD/AgNPs nanocomposite at the nanoscale. The coexistence of crystalline silver phases and amorphous carbon components verifies the hybrid nature of the material. The uniform morphology and nanoscale dimensions provide a high surface-area-to-volume ratio, facilitating effective contact and interaction between the nanocomposite and

View Article Online
DOI: 10.1039/D5MA00802F

microbial cells—an important factor contributing to the antibacterial performance discussed in the following section.

### 3.2. Antibacterial Activity

The minimum inhibitory concentration (MIC) values of the CQD/AgNPs nanocomposite against five ESKAPEE bacterial strains are shown in Table 1. These strains—including *Acinetobacter baumannii, Pseudomonas aeruginosa, Klebsiella pneumoniae, Escherichia coli*, and *Staphylococcus aureus*—are well-known clinical pathogens with high resistance to antibiotics, strong biofilm-forming abilities, and frequent association with hospital-acquired infections.

Notably, *A. baumannii* and *P. aeruginosa* are major causes of severe pneumonia and bloodstream infections in intensive care units (ICUs), often resistant to nearly all conventional antibiotics, including carbapenems. *K. pneumoniae* and *E. coli*, though more common, are rapidly acquiring resistance to fluoroquinolones and β-lactams. Meanwhile, S. aureus, especially methicillin-resistant strains (MRSA), remains a persistent threat both in community and healthcare settings.

As shown in Table 1, the CQDs/AgNPs nanocomposite exhibited noticeable antibacterial activity, with MIC values ranging from 25 to 50 μg $mL^{-1}$. In particular, A. baumannii—a WHO-prioritized multidrug-resistant pathogen—was completely inhibited at 25 μg $mL^{-1}$, suggesting a relatively strong antibacterial effect. The other strains (P. aeruginosa, K. pneumoniae, E. coli, and S. aureus) were inhibited at 50 μg $mL^{-1}$, indicating broad-spectrum activity.

*Table 1: Minimum inhibitory concentration values of the as-synthesized CQDs and CQD/AgNPs*

| **Sample** | **MIC (μg $mL^{-1}$)** ***Escherichia coli ND01*** | **MIC (μg $mL^{-1}$)** ***Staphylococcus aureus (MRSA) VS02*** | **MIC (μg $mL^{-1}$)** ***Klebsiella pneumoniae VS39*** | **MIC (μg $mL^{-1}$)** ***Acinetobacter baumannii VS73*** | **MIC (μg $mL^{-1}$)** ***Pseudomonas aeruginosa ND26*** |
|---|---|---|---|---|---|
| CQDs | >1000 | >1000 | >1000 | >1000 | >1000 |

View Article Online
DOI: 10.1039/D5MA00802F

| | | | | | |
|---|---|---|---|---|---|
| CQD/AgNPs | 50 | 50 | 50 | 25 | 50 |
| **Ciprofloxacin** | 64 | 128 | 0.5 | 128 | 64 |

For comparison, the MICs of ciprofloxacin against the same strains ranged from 0.5 to 128 μg $mL^{-1}$, with A. baumannii and K. pneumoniae showing particularly high resistance (128 μg $mL^{-1}$). These findings imply that the CQD/AgNPs nanocomposite possesses a promising antibacterial potential, especially toward resistant A. baumannii. The enhanced performance may arise from the combined effects of CQDs and AgNPs, which help stabilize the nanoparticles, facilitate $Ag^{+}$ release, and promote ROS generation at the bacterial interface.

To further verify the possible synergistic effect between CQDs and AgNPs, additional comparative antibacterial assays were conducted under identical conditions. The results demonstrated that CQDs alone showed negligible activity (MIC > 1000 μg $mL^{-1}$), AgNPs alone had an MIC of 50 μg $mL^{-1}$, whereas the CQDs/AgNPs composite exhibited a markedly enhanced activity with an MIC of 25 μg $mL^{-1}$ against A. baumannii as summarized in Table 2. Consistently, the inhibition zone increased from 14 mm (AgNPs) to 17 mm (CQDs/AgNPs). To quantitatively evaluate the interaction between CQDs and AgNPs, the fractional inhibitory concentration (FIC) index was employed as a standard method for determining synergistic effects in antimicrobial combinations. The FIC index is calculated based on the minimum inhibitory concentrations of individual agents and their combinations, providing an objective measure of whether the interaction is synergistic (FIC ≤ 0.5), additive (0.5 < FIC ≤ 1), indifferent (1 < FIC ≤ 4), or antagonistic (FIC > 4) (39).

$$\text{FIC} = \left(\frac{MIC\ A_{combination\ A\&B}}{MIC_{agent A}}\right) + \left(\frac{MIC\ B_{combination\ A\&B}}{MIC_{agent\ B}}\right)$$

Applying the standard FIC formula, the calculated value was 0.53, slightly above the conventional synergistic threshold (≤ 0.5). Therefore, this result indicates a near-synergistic interaction, meaning that the presence of CQDs effectively enhances the antibacterial performance of the composite.

*Table 2: Minimum inhibitory concentration and growth inhibition diameter values of the as-synthesized CQDs, AgNPs and CQD/AgNPs*

| **Sample** | **MIC** (μg $mL^{-1}$) | **ZOI** (mm) |
|---|---|---|

View Article Online
DOI: 10.1039/D5MA00802F

| | | |
|---|---|---|
| **CQDs** | >1000 | --- |
| **AgNPs** | 50 | 14±2 |
| **CQD/AgNPs** | 25 | 17±2 |

Building upon these findings, a comparative overview between our synthesized CQD/AgNPs nanocomposite and other previously reported green-synthesized nanomaterials in terms of antibacterial activity against Acinetobacter baumannii is summarized in Table 3.

*Table 3: MIC values of green-synthesized nanomaterials against Acinetobacter baumannii.*

| **Material** | **MIC (μg mL⁻¹)** | **Ref** |
|---|---|---|
| AgNPs (Ginkgo) | 8 | (16) |
| **CQD/AgNPs (Guava)** | **25** | **This study** |
| AgNPs (Ocimum sanctum Linn) | 32 | (40) |
| AgNPs | 62.5 | (41) |
| CQD/AgNPs | 234 | (19) |
| AgNPs | 125 | (42) |
| AgNPs (curcumin) | 250 | (17) |
| AgNPs (Acroptilon) | 50-400 | (43) |
| Monsonia Angustifolia and Momordica Balsamina Linn Extracts | 500 | (44) |

Table 3 shows that individual plant extracts, such as those from Psidium guajava or other medicinal plants, generally exhibit only limited intrinsic antibacterial activity against multidrug-resistant (MDR) bacterial strains, particularly *Acinetobacter baumannii*. Crude plant-based formulations, such as the combination of extracts from *Monsonia angustifolia* and *Momordica balsamina Linn*, require high minimum inhibitory concentrations (MICs),

View Article Online
DOI: 10.1039/D5MA00802F

around 500 μg $mL^{-1}$, to suppress bacterial growth, reflecting their weak inherent antimicrobial potency (44).

In contrast, when phytochemicals are used as reducing and stabilizing agents during the synthesis of silver nanoparticles (AgNPs), the resulting nanocomposites often show significantly enhanced antibacterial performance. Among reported green-synthesized AgNP systems, the strongest activity was observed in AgNPs derived from Ginkgo biloba, with MIC values as low as 8 μg $mL^{-1}$ (16). Other systems, such as AgNPs synthesized from Ocimum sanctum (MIC = 32 μg $mL^{-1}$) (40) , Acroptilon extracts (MIC ranging from 50 to 400 μg $mL^{-1}$) (43) and *Monsonia Angustifolia* and *Momordica Balsamina Linn* Extracts (MIC = 500 μg $mL^{-1}$) (44) also demonstrated improved antibacterial effects although with considerable variability depending on synthesis conditions and particle uniformity.

In our study, the CQD/AgNPs nanocomposite exhibited an MIC of 25 μg $mL^{-1}$ against the carbapenem-resistant *A. baumannii* strain. Although this MIC is slightly higher than that of the most potent Ginkgo-derived AgNPs, it remains within the effective therapeutic range and outperforms many other green-synthesized materials. Notably, our nanocomposite was synthesized via a fully green method, free of toxic chemicals. This approach yielded a colloidally stable material that retains functionality over time at room temperature, eliminating the need for refrigerated storage. The combination of long-term room temperature stability, the use of abundant and locally available biomass feedstock, and a synthesis method that is scalable makes our nanocomposite a promising candidate for industrial-scale production.

To visually illustrate the antibacterial efficacy of the CQD/AgNPs nanocomposite (sample M1), we performed zone of inhibition (ZOI) assays against four clinically isolated multidrug-resistant (MDR) bacterial strains, namely Escherichia coli, Klebsiella pneumoniae, Acinetobacter baumannii, and Pseudomonas aeruginosa, as shown in Figure 7. These ESKAPEE group strains were isolated from clinical specimens at the University Medical Center in Ho Chi Minh City (UMC-HCMC) and were confirmed to be resistant to ciprofloxacin as well as several other commonly used antibiotics

View Article Online
DOI: 10.1039/D5MA00802F

As shown in Figure 7, *E. coli, A. baumannii*, *and P. aeruginosa* showed no measurable inhibition zones with ciprofloxacin, confirming their resistance. In contrast, sample M1 displayed clear antibacterial activity, with ZOI diameters of 15 mm, 17 mm, and 17 mm, respectively. For *K. pneumoniae*, ciprofloxacin (30 µg $mL^{-1}$) still produced a large inhibition zone of 30 mm, while M1 showed a smaller ZOI of about 13 mm. Nevertheless, M1 demonstrated broad-spectrum antibacterial activity across multiple ESKAPEE strains. These findings highlight the potential of the CQD/AgNPs nanocomposite as an alternative antimicrobial agent against multidrug-resistant bacteria, with possible applications as a disinfectant or hand sanitizer for healthcare workers.

*Table 4: Growth inhibition diameter value of the antibiotic plates and silver nanocomposites (M1) against ESKAPEE isolates*

| Test ESKAPEE | Ciprofloxacin | M1 (CQD/AgNPs) |
|---|---|---|
| *Escherichia coli* | --- | 15 ± 2 mm |
| *Klebsiella pneumoniae* | 30 mm ± 2 mm | 13 ± 2 mm |
| *Acinetobacter baumannii* | --- | 17 ± 2 mm |
| *Pseudomonas aeruginosa* | --- | 17 ± 2 mm |

View Article Online
DOI: 10.1039/D5MA00802F



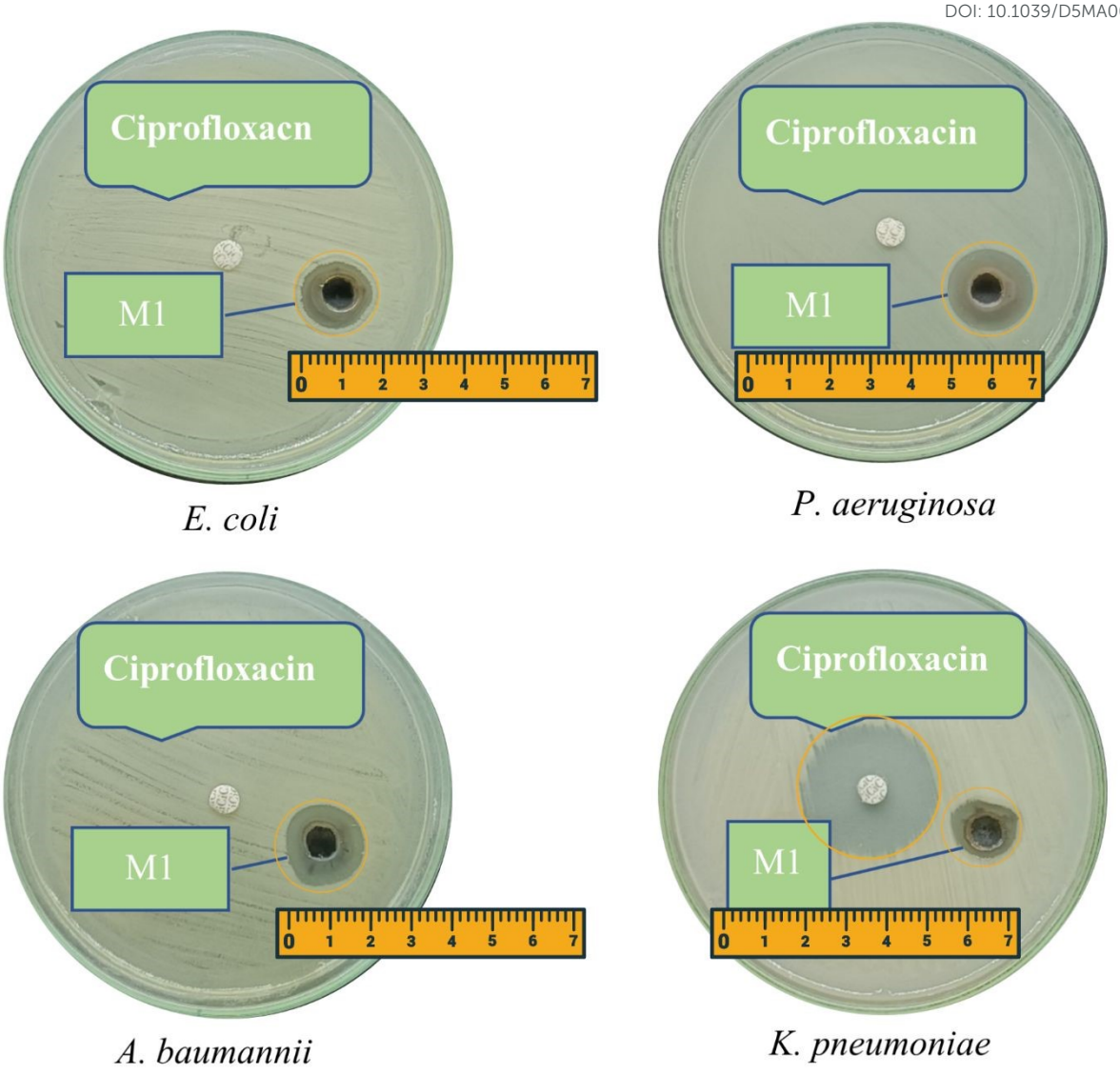


*Figure 7: Images of Inhibition zone of the antibiotic plates and CQD/AgNPs nanocomposite against ESKAPEE pathogens.*

The remarkable antibacterial activity of the CQD/AgNPs composite can be attributed to the combined contributions of carbon quantum dots and silver nanoparticles. The well-dispersed AgNPs continuously release $Ag^+$ ions, which interact with bacterial cell walls and intracellular components, leading to membrane disruption and cell death, as illustrated in Fig. 8. Meanwhile, the CQDs provide abundant surface functional groups (–COOH, –OH, $–NH_2$) that enhance the adhesion of the composite to bacterial membranes, improve dispersion stability, and facilitate reactive oxygen species (ROS) generation. In addition, the presence of CQDs helps stabilize the AgNPs, increase the effective contact surface

View Article Online
DOI: 10.1039/D5MA00802F

area, and promote better nanoparticle dispersion, thereby allowing $Ag^+$ ions to interact more efficiently with bacterial cells. These combined effects increase oxidative stress, enhance membrane permeability, and ultimately result in efficient bacterial inactivation (21).

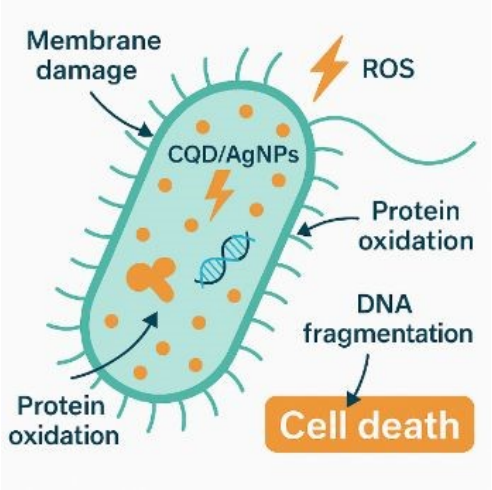


*Figure 8: The probable mechanism of the antibacterial activity of CQD/AgNP nanocomposite*

To evaluate its potential for future biomedical applications, a preliminary cytotoxicity test was performed on the CQD/AgNPs nanocomposite using the standard MTT assay on HEK293A cells.

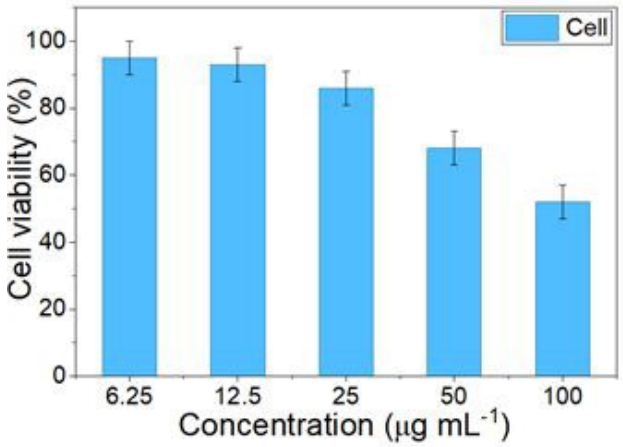


*Figure 9: Relative viability of HEK293A cells treated with different concentrations of CQD/AgNPs for 24 h.*

As shown in Fig. 9, the cells were treated with different concentrations of the nanocomposite (100, 50, 25, 12.5, and 6.25 μg $mL^{-1}$) for 24 h. The percentage of viable cells was calculated relative to the untreated control based on the absorbance of the formazan product measured at 570 nm.

View Article Online
DOI: 10.1039/D5MA00802F

The results showed a concentration-dependent reduction in cell viability, however, the viability remained above 70% at concentrations of 50 μg $mL^{-1}$ and 25 μg $mL^{-1}$. This indicates that the CQD/AgNPs nanocomposite exhibits acceptable cytocompatibility at these working concentrations. These findings suggest that the material could serve as a promising candidate for the future development of antimicrobial nanomaterials or next-generation antibiotic alternatives.

## Conclusion

In this study, we developed a cost-effective, green-synthesized CQD/AgNPs nanocomposite using Psidium guajava leaf extract, which served as both the carbon source and a natural reducing agent. The incorporated CQDs further enhanced the antibacterial performance of the composite by improving nanoparticle dispersion, stabilizing AgNPs, and contributing additional surface functional groups that promote membrane interaction and reactive oxygen species (ROS) generation.The resulting material exhibited strong antibacterial activity against multidrug-resistant (MDR) ESKAPEE pathogens, with a minimum inhibitory concentration (MIC) of 25 μg $mL^{-1}$ against *Acinetobacter baumannii*. Structural characterization confirmed the formation of stable and uniformly dispersed nanoparticles. Importantly, the nanocomposite remained stable at room temperature for at least six months without the need for refrigeration, offering a practical advantage for storage and potential scale-up. In conclusion, these results suggest that the synthesized CQD/AgNPs nanocomposite is not only environmentally friendly and biocompatible but also a promising alternative for future antimicrobial applications.

## Author Contribution

Hoang Thi Thu: Conceptualization; Methodology; Data curation; Formal analysis ; Writing – original draft ; Writing – review & editing; Supervision.

Le Tuan Anh: Resources; Validation; Investigation; Formal analysis

Dang Thien Huong: Investigation ; Visualization; Data curation; Writing – original draft

Duong Ngoc Huyen: Project administration; Supervision.

## Data availability statement

All data supporting the findings of this study are available within the article and its supplementary information files.

View Article Online
DOI: 10.1039/D5MA00802F

## Conflict of interest

The authors declare that there are no conflicts of interest to declare.

## Acknowledgements

The authors would like to thank the Industrial University of Ho Chi Minh City (IUH) for providing laboratory facilities and technical support for this research.

## References

1. Daruka L, Czikkely MS, Szili P, Farkas Z, Balogh D, Grézal G, et al. ESKAPE pathogens rapidly develop resistance against antibiotics in development in vitro. Nat Microbiol. 2025 Jan 13;10(2):313–31.

2. Ibrahim SI, Parambil AM, Jha N, Tomar AK, Rajamani P, Jian X, et al. Targeting ESKAPE pathogens with ZnS and Au@ZnS Core–Shell nanoconjugates for improved biofilm control. Sci Rep [Internet]. 2025 July 1 [cited 2025 July 13];15(1). Available from: https://www.nature.com/articles/s41598-025-07583-5

3. Salam MdA, Al-Amin MdY, Salam MT, Pawar JS, Akhter N, Rabaan AA, et al. Antimicrobial Resistance: A Growing Serious Threat for Global Public Health. Healthcare. 2023 July 5;11(13):1946.

4. Antimicrobial resistance in the EU/EEA (EARS-Net) - Annual epidemiological report for 2023. 2023;

5. Karnwal A, Jassim AY, Mohammed AA, Al-Tawaha ARMS, Selvaraj M, Malik T. Addressing the global challenge of bacterial drug resistance: insights, strategies, and future directions. Front Microbiol [Internet]. 2025 Feb 24 [cited 2025 July 13];16. Available from: https://www.frontiersin.org/articles/10.3389/fmicb.2025.1517772/full

6. Mulani MS, Kamble EE, Kumkar SN, Tawre MS, Pardesi KR. Emerging Strategies to Combat ESKAPE Pathogens in the Era of Antimicrobial Resistance: A Review. Front Microbiol. 2019 Apr 1;10:539.

7. Rox K, Medina E. Aerosolized delivery of ESKAPE pathogens for murine pneumonia models. Sci Rep [Internet]. 2024 Jan 31 [cited 2025 July 13];14(1). Available from: https://www.nature.com/articles/s41598-024-52958-9

8. Rodrigues AS, Batista JGS, Rodrigues MÁV, Thipe VC, Minarini LAR, Lopes PS, et al. Advances in silver nanoparticles: a comprehensive review on their potential as antimicrobial agents and their mechanisms of action elucidated by proteomics. Front Microbiol. 2024 July 31;15:1440065.

9. Ren Y, Zhang Y, Li X. Application of AgNPs in biomedicine: An overview and current trends. Nanotechnol Rev. 2024 July 1;13(1):20240030.

View Article Online
DOI: 10.1039/D5MA00802F

10. Al-Gburi N, Al-Hassnawi A, Al-Bayati LA. Biosynthesis of Silver Nanoparticles and Their Roles in the Biomedical Field: A Review. Med J Babylon. 2024 July;21(3):493–9.

11. Kumar L, Bisen M, Harjai K, Chhibber S, Azizov S, Lalhlenmawia H, et al. Advances in Nanotechnology for Biofilm Inhibition. ACS Omega. 2023 June 20;8(24):21391–409.

12. Chartarrayawadee W, Charoensin P, Saenma J, Rin T, Khamai P, Nasomjai P. Green synthesis and stabilization of silver nanoparticles using Lysimachia foenum-graecum Hance extract and their antibacterial activity.

13. Musthafa M. Antibacterial Activity of Wound Healing Spacer Materials Coated with Green Synthesized AgNP-AMP Conjugates against "ESKAPE" Members of Clinical Isolates from Different Types of Wounds. J Res Med Dent Sci. 2021;9(4).

14. Giri AK, Jena B, Biswal B, Pradhan AK, Arakha M, Acharya S, et al. Green synthesis and characterization of silver nanoparticles using Eugenia roxburghii DC. extract and activity against biofilm-producing bacteria. Sci Rep [Internet]. 2022 May 19 [cited 2025 July 14];12(1). Available from: https://www.nature.com/articles/s41598-022-12484-y

15. Mikhailova EO. Green Silver Nanoparticles: An Antibacterial Mechanism. Antibiotics. 2024 Dec 25;14(1):5.

16. Ni Q, Zhu T, Wang W, Guo D, Li Y, Chen T, et al. Green Synthesis of Narrow-Size Silver Nanoparticles Using Ginkgo biloba Leaves: Condition Optimization, Characterization, and Antibacterial and Cytotoxic Activities. Int J Mol Sci. 2024 Feb 5;25(3):1913.

17. Abdelwahab MA, Nabil A, El-Hosainy H, Tahway R, Taha MS. Green synthesis of silver nanoparticles using curcumin: A comparative study of antimicrobial and antibiofilm effects on Acinetobacter baumannii against chemical conventional methods. Results Chem. 2024 Jan;7:101274.

18. Raza S, Wdowiak M, Grotek M, Adamkiewicz W, Nikiforow K, Mente P, et al. Enhancing the antimicrobial activity of silver nanoparticles against ESKAPE bacteria and emerging fungal pathogens by using tea extracts. Nanoscale Adv. 2023;5(21):5786–98.

19. El Ghacham S, Hejji L, Aoulad El Hadj Ali Y, Wahby A, Tamegart L, Pérez-Villarejo L, et al. Enhanced antibacterial and wound healing efficacy of a novel CQDs@AgNPs@CS-based nanocomposites: A multifunctional approach for advanced wound care. Int J Biol Macromol. 2025 June 1;311:143621.

20. Liu T, Pang Q, Mai K, He X, Xu L, Zhou F, et al. Silver nanoparticle@carbon quantum dot composite as an antibacterial agent. RSC Adv. 2022;12(16):9621–7.

View Article Online
DOI: 10.1039/D5MA00802F

21. El Ghacham S, Hejji L, Aoulad El Hadj Ali Y, Azzouz A, Pérez-Villarejo L, Tamegart L, et al. Green-synthesized carbon quantum dots–silver nanocomposites for broad-spectrum antimicrobial and wound healing applications. J Drug Deliv Sci Technol. 2025 June 1;108:106964.

22. Jia J, Sun Y, Zhang Y, Liu Q, Cao J, Huang G, et al. Facile and Efficient Fabrication of Bandgap Tunable Carbon Quantum Dots Derived From Anthracite and Their Photoluminescence Properties. Front Chem. 2020 Feb 28;8:123.

23. Sheshmani S, Mardali M, Shokrollahzadeh S, Bide Y, Tarlani R. Synthesis, optical, and photocatalytic properties of cellulose-derived carbon quantum dots. Sci Rep [Internet]. 2025 May 30 [cited 2025 July 13];15(1). Available from: https://www.nature.com/articles/s41598-025-04453-y

24. Kumar M, Chinnathambi S, Bakhori N, Abu N, Etezadi F, Thangavel V, et al. Biomass-derived carbon dots as fluorescent quantum probes to visualize and modulate inflammation. Sci Rep [Internet]. 2024 June 3 [cited 2025 July 14];14(1). Available from: https://www.nature.com/articles/s41598-024-62901-7

25. Ateia EE, Rabie O, Mohamed AT. Assessment of the correlation between optical properties and CQD preparation approaches. Eur Phys J Plus. 2024 Jan 6;139(1):24.

26. Kaur R, Singh J, Kathuria D, Matharu AS. Waste biomass-derived CQDs and Ag-CQDs as a sensing platform for Hg2+ ions. Sustain Chem Pharm. 2022 Oct 1;29:100813.

27. Praseetha PK, Litany RIJ, Alharbi HM, Khojah AA, Akash S, Bourhia M, et al. Green synthesis of highly fluorescent carbon quantum dots from almond resin for advanced theranostics in biomedical applications. Sci Rep [Internet]. 2024 Oct 18 [cited 2025 July 14];14(1). Available from: https://www.nature.com/articles/s41598-024-75333-0

28. Amirsoleimani A, Bahrami Z, Abdoos H, Kafshdouzan K. Synthesis and characterization of Zn-doped carbon dots derived from calendula officinalis and glucose: Antibacterial and photoluminescence properties. Carbon Trends. 2025 Aug;20:100537.

29. Ghirardello M, Ramos-Soriano J, Galan MC. Carbon Dots as an Emergent Class of Sustainable Antifungal Agents. ACS Nano. 2025 July 2;19.

30. Diab EA, Ghali M, Mosaad MM. In vitro antimicrobial and anticancer potentials of green synthesized luminescent carbon quantum dots derived from artichoke leaves. Sci Rep [Internet]. 2025 May 9 [cited 2025 July 18];15(1). Available from: https://www.nature.com/articles/s41598-025-99841-9

31. Saravanan A, Das P, Maruthapandi M, Aryal S, Michaeli S, Mastai Y, et al. Heteroatom co-doping (N, NS, NB) on carbon dots and their antibacterial and antioxidant properties. Surf Interfaces. 2024 Mar 1;46:103857.

View Article Online
DOI: 10.1039/D5MA00802F

32. Saravanan A, Maruthapandi M, Das P, Ganguly S, Margel S, Luong JHT, et al. Applications of N-Doped Carbon Dots as Antimicrobial Agents, Antibiotic Carriers, and Selective Fluorescent Probes for Nitro Explosives. ACS Appl Bio Mater. 2020 Nov 16;3(11):8023–31.

33. Zarouki MA, Tamegart L, Hejji L, El Hadj Ali YA, Ayadi AE, Villarejo LP, et al. Graphene quantum dots based on cannabis seeds for efficient wound healing in a mouse incisional wound model: Link with stress and neurobehavioral effect. Int J Pharm. 2024 Jan 5;649:123658.

34. Peng J, Gao W, Gupta B, Liu Z, Romero Aburto R, Ge L, et al. Graphene Quantum Dots Derived from Carbon Fibers. Nano Lett. 2012 Jan 4;12:844–9.

35. Shen F, Lu Z, Yan K, Luo K, Pei S, Xiang P. Synthesis and properties of carbon quantum dots as an antimicrobial agent and detection of ciprofloxacin. Sci Rep. 2025 Aug 5;15(1):28535.

36. Li Z, Deng L, Kinloch IA, Young RJ. Raman spectroscopy of carbon materials and their composites: Graphene, nanotubes and fibres. Prog Mater Sci. 2023 June;135:101089.

37. Dong Y, Wang Q, Wan L, You X, Chi Y. Carbon based dot capped silver nanoparticles for efficient surface-enhanced Raman scattering. J Mater Chem C. 2016;4(31):7472–7.

38. Salman BI. Synthesis of highly fluorescent green carbon quantum dots from Prunus armeniaca for the determination of lisinopril in human plasma. Sci Rep. 2025 Sept 12;15(1):32502.

39. Doern CD. When Does 2 Plus 2 Equal 5? A Review of Antimicrobial Synergy Testing. Carroll KC, editor. J Clin Microbiol. 2014 Dec;52(12):4124–8.

40. Gautam D, Dolma KG, Khandelwal B, Gupta M, Singh M, Mahboob T, et al. Green synthesis of silver nanoparticles using *Ocimum sanctum* Linn. and its antibacterial activity against multidrug resistant *Acinetobacter baumannii*. PeerJ. 2023 July 28;11:e15590.

41. Kakian F, Arasteh N, Mirzaei E, Motamedifar M. Study of MIC of silver and zinc oxide nanoparticles, strong and cost-effective antibacterial against biofilm-producing Acinetobacter baumannii in Shiraz, Southwest of Iran. BMC Infect Dis. 2024 June 17;24(1):593.

42. Ahmed MS, Abdulrahman ZirakFA, Taha ZMA. The effect of silver nanoparticles on the antimicrobial activity of cloned nisin against extensively drug-resistant Acinetobacter baumannii". J Infect Public Health. 2024 Sept;17(9):102501.

View Article Online
DOI: 10.1039/D5MA00802F

43. Shamsoddini S, Davoudi M, Shahbazi S, Zare Karizi S. Green synthesis of silver nanoparticles using Acroptilon repens aqueous extract and their antibacterial efficacy against multidrug-resistant Acinetobacter baumannii. Mol Biol Rep. 2024 Dec;52.

44. Nogbou ND, Mabela DR, Matseke B, Mapfumari NS, Mothibe ME, Obi LC, et al. Antibacterial Activities of Monsonia Angustifolia and Momordica Balsamina Linn Extracts against Carbapenem-Resistant Acinetobacter Baumannii. Plants. 2022 Sept 12;11(18):2374.



View Article Online
DOI: 10.1039/D5MA00802F

## Data availability statement

All data supporting the findings of this study are available within the article and its supplementary information files.